IEEE Access
Multidisciplinary | Rapid Review | Open Access Journal

Date of publication xxxx 00, 0000, date of current version xxxx 00, 0000.

Digital Object Identifier 10.1109/ACCESS.2024.Doi Number

Dynamic Fuzzy Logic Energy Management System for a Multi-Energy Microgrid

Pablo Horrillo-Quintero[1], Pablo García-Triviño[1], Ehsan Hoseinni[1], Carlos Andrés García-Vázquez[1], Higinio Sánchez-Sainz[2] (Senior Member, IEEE), Carlos E. Ugalde-Loo[3] (Senior Member, IEEE), Vedran Peric[4] (Member, IEEE), Luis M. Fernández-Ramírez[1] (Senior Member, IEEE).

[1] Research Group in Sustainable and Renewable Electrical Technologies – SURET (PAIDI-TEP023), Department of Electrical Engineering, University of Cadiz (UCA), ETSI Algeciras, 11202 Algeciras (Cádiz), Spain
[2] Research Group in Sustainable and Renewable Electrical Technologies – SURET (PAIDI-TEP023), Department of Electrical Engineering, University of Cadiz (UCA), ESI Puerto Real, 11202 Algeciras (Cádiz), Spain
[3] School of Engineering, Cardiff University, Cardiff CF24 3AA, UK.
[4] Department of Electrical and Computer Engineering, Aarhus University, 8200 Aarhus N, Denmark

Corresponding author: Luis M. Fernández-Ramírez (e-mail: luis.fernandez@uca.es).

This work was partially supported by Ministerio de Ciencia e Innovación, Agencia Estatal de Investigación, and Unión Europea "NextGenerationEU"/PRTR" (Grant TED2021-129631B-C32 supported by MCIN/AEI/10.13039/501100011033 and NextGenerationEU/PRTR).

ABSTRACT While multi-energy microgrids (MEMGs) offer a promising approach to reduce energy consumption through coordinated integration of various energy vectors, research has primarily focused on static studies. These studies aim to optimize a particular cost function but neglect the dynamic aspects of the system operation. This paper presents a dynamic model of an MEMG comprising of electricity and thermal vectors. A novel dynamic fuzzy logic-based energy management system (EMS) is investigated, aiming to ensure energy balance (electric and thermal), optimize renewable energy utilization, and reduce the reliance on the local electricity grid and gas. Both the EMS and MEMG have been evaluated under different weather conditions and a 4-hour variable load profile. Furthermore, the EMS effectiveness has been verified through a real-time experiment using an OPAL-RT4512 unit and a dSPACE MicroLabBox prototype. The results show that the proposed fuzzy logic-based EMS outperforms a conventional EMS based on machine states (states-based EMS), achieving a notable reduction in electricity grid consumption of 80%, as well as a consumption reduction of 7.4% in the gas boiler and 5.4% in the electric boiler. Furthermore, the control performance results in a remarkable reduction in ITAE (42.57%), ITSE (89.10%), IAE (54.36%) and ISE (57.55%) for the hot water temperature control, and in ITAE (17.06%), ITSE (52.50%), IAE (31.19%) and ISE (29.99%) for the heating control.

INDEX TERMS Electricity, energy management system, energy storage system, fuzzy-logic, multi-energy microgrids, thermal

I. INTRODUCTION

The push to increase the energy efficiency in electricity networks is driving the advancement of distributed generation through microgrids (MGs) that incorporate renewable energy sources with energy storage systems (ESSs) to address their variability. It is possible to include multiple energy vectors in a MG, such as electricity, heat/cooling, gas or hydrogen to build a multi-energy microgrid (MEMG) [1,2].

A MEMG considers multiple energy vectors with a complementary relationship that improves the efficiency of the whole system [3,4], carrying out a multi-objective operation.

Multi-objective operation typically aims to minimize the total operational cost of the microgrid system, improve energy balance, and enhance overall system performance [5].

Traditionally, the study of MEMGs has focused on static analysis, examining the MEMG response at a single point in time to assess its current state or predict its future state. However, this approach overlooks the dynamic behavior and real-time response of MEMGs, limiting the understanding of how they respond to changes over time.

The main idea of a steady-state study is to optimize a cost or efficiency-related objective function [6]-[8].

For instance, a model minimizing the carbon footprint of an energy community was introduced in [9]. MEMG optimization problems are commonly solved using mixed-integer linear programming (MILP) with alternating directional multiplier method [10].

The research conducted in [11] concentrated on the integration of electric-thermal power flow using an extended Newton-Raphson algorithm. Furthermore, an optimization model for MEMGs was implemented in [12] using a MILP approach for a corrective receding horizon considering costs, emissions, and flexibility, through optimization over annual and daily time horizons. Several studies [13-14] pointed out the optimization of MEMGs in long term time horizon and muti-time scale.

MEMGs represent an efficient solution for both grid-connected and islanded operation modes. In [15], an algorithm was introduced to optimize planning decisions, enhance operating costs in grid-connected mode, and increase supply reliability in islanded mode. This approach accounts for uncertainties in both demand and renewable production.

Energy storage is an imperative need for mitigating fluctuations in renewable production. In [16], it was demonstrated that storage systems can lead to cost savings in MEMG operations and reduced losses through Mixed Integral Linear Programming technique.

The steady-state solutions hold under the assumption that the MEMG works within an operating range closely resembling the one studied [17-19]. In [20], an optimization cooperative demand-driven operational approach for a MEMG was presented, comprising a higher-level model and a lower-level model. However, the optimization was enclosed to the constraints and might not be adequate in different operating conditions. In [21], the demand problem was studied with nonlinear integrated demand response system for MEMGs based on pricing, aimed at mitigating errors in estimating both electricity and gas loads. However, this study did not explore real-time implementation of these scenarios.

The static optimization presented in [22], employed demand management in two stages. The initial phase of optimization focused on employing a mixed-integer nonlinear programming approach to maximize projected profits from day-ahead operations. Subsequently, the second phase of the energy management plan aimed to minimize anticipated costs for hour-ahead operations. However, no details were provided regarding the dynamic behavior of the MEMG during the optimization processes, and the models used may not be suitable beyond the studied linearization point.

In [23], total operating costs were minimized considering uncertainties in renewable production, demand, and energy prices. In this scenario, the system operator has the opportunity to actively engage in electricity, heat, and gas markets, enabling them to meet local energy demands and maximize profits through energy exchanges.

To expand the operational capabilities of MEMGs and effectively manage dynamic conditions, the development of dynamic model is crucial. This allows the operation, control, and energy management system (EMS) to adapt to weather variations and sudden demand changes. Consequently, a more efficient distribution of energy between MEMG components becomes possible.

A dynamic EMS incorporates instantaneous monitoring and control of energy consumption, considering temporary operating modes [24]. It has the ability to react to real-time fluctuations in demand by adjusting production levels, considering weather conditions and the state-of-charge (SOC)

NOMENCLATURE

c	Heat capacity boiler (J/(kg·K))
C_B	Thermal capacity of the electric boiler (J/K)
c_{f}	Heat capacity of fluid (J/(kg·K))
c_{p}	Heat capacity of fluid (const. pressure) (J/(kg·K))
E_{BESS}	BESS open circuit voltage (V)
G_s, G_n	Irradiation on the surface and the nominal irradiation
I_{BESS}	BESS current (A)
I_{PV}	PV current (A)
I_L, I_{L0}	Light current and light current at SRC (A)
I_{sat}	Diode reverse saturation current (A)
k	Boltzmann's constant (1.38066×10^{-23} J/K)
K_0, K_1	Constants depending on the PV characteristic
m	Mass of the boiler (kg)
$\dot{m}_{bus}$	Mass flow rate in the thermal bus (kg/s)
$\dot{m}_{water}$	Mass flow water demand (kg/s)
N	Number of nodes
N_s	Number of cells in series
P_{BESS}	BESS power (W)
$P_{BESS,dis}^{max}$	Maximum BESS power in discharging (W)
$P_{BESS,cha}^{max}$	Maximum BESS power in charging (W)
P_{EB}	Electric boiler power (W)
P_{GRID}	Local grid power (W)
P_{LOAD}	Electric load power (W)
P_{PV}	PV power (W)
P'_{NET}	Gross net power (W)
P_{NET}	Net power (W)
q	Electron charge (1.60218E–19 Coulomb)
Q_{EB}	Heat power of the electric boiler (W)
Q_{GB}	Heat power of the gas boiler (W)
Q_{EB}^{out}	Heat extracted by the electric boiler (W)
R_{int}	BESS internal resistance (Ω)
R_s, R_{sh}	Series and shunt resistance (Ω)
T_{amb}	Ambient temperature (ºC)
$T_{\mathrm{bus}}, T_{bus}^{ref}$	Bus temperature and reference bus temperature(ºC)
T_{EB}	Electric boiler temperature (ºC)
T_{in}	Temperature of fluid at the input (ºC)
$T_{EB}^{max}, T_{EB}^{min}$	Electric boiler turns off/on temperature (ºC)
T_2	Temp. after electric boiler heat exchange (ºC)
T_{PV}	Photovoltaic cell temperature (ºC)
UA	Heat loss coefficient to ambient (W/K)
V_{BESS}	BESS voltage (V)
V_g	Diode voltage (V)

of the energy storage systems (ESSs). By implementing this dynamic approach, MEMGs can achieve optimal performance across diverse operating conditions, leading to maximized efficiency and minimized operational costs.

As evidenced in the existing literature, most studies have largely overlooked the dynamic nature of MEMGs, leading to a significant research gap in the dynamic control of MEMGs facilitated by an EMS.

The approach to energy control and management in MEMG studies requires dynamic models capable of accurately representing equipment behavior across various operating points, and effectively responding to changes in operating conditions. In complex MEMGs incorporating diverse renewable generation equipment, energy storage and thermal sources, designing an EMS becomes a challenging task, requiring intelligent techniques for efficient energy management [25]. This challenge involves addressing several system operator objectives concurrently, such as minimizing energy supply from the main grid while controlling ESS charge levels.

Among the different intelligent techniques presented in the literature, fuzzy logic control is a widely adopted approach for dynamic EMSs. Fuzzy logic systems have gained extensive popularity across diverse fields owing to their inherent ability to be used in complex systems. Unlike other intelligent controllers that heavily rely on historical data, fuzzy systems do not require such data to function effectively. Furthermore, fuzzy logic control eliminates the need for system linearization, further simplifying its application in dynamic models [26].

In traditional energy systems, electric and thermal systems have been designed, planned, and operated independently, despite their physical complementarity. In the quest to optimize energy usage and integrate renewable energy-based generation systems and energy storage systems, there is a growing need to interconnect electricity systems and coordinate their operation with other energy vectors, such as heat, taking into account the control approach to achieve this.

Current literature has not adequately addressed the study of MEMGs from the perspective of real-time control, as well as EMS that integrate different energy vectors. Both operators of electric and thermal grid systems, as well as operators of distributed generation, require real-time control to integrate renewable energy sources into residential networks that consume various types of energy in a safe and efficient manner. Similarly, end-users benefit from having efficient energy control and management systems, giving them greater decision-making capabilities based on available capacity and demand.

There are deficiencies on the design of interconnected real-time energy control and management systems, while considering various reliability, resilience, and efficiency indicators within MEMGs. Additionally, minimizing energy consumption, taking into account the savings associated with harnessing the flexibility offered by ESS in MEMGs, is a pressing need due to the intrinsic intermittency of renewable generation. This problem is further exacerbated if there are heat-generating devices powered by renewable-produced electricity. Controlled real-time exchange of surplus non-dispatchable and dispatchable generation between different energy vectors is a fundamental issue for integrating RET and ESS into current distribution networks.

This paper addresses this gap by presenting an MEMG considering electricity and thermal vectors controlled by a novel dynamic fuzzy logic-based EMS acting as a supervisory controller for the entire system. The primary objective of the EMS is to minimize energy withdrawal from the local grid and maximize the utilization of renewable energy sources while meeting the electrical and thermal demands. The innovative aspect of this paper lies in determining the operating mode of the thermal sources, and the management of the battery ESS (BESS) based on the real-time thermal and electric demands, renewable energy availability and the SOC of the BESS.

The contributions of this paper are summarized as follows:

- Dynamic control management (with a sample time of 0.02s) for a MEMG with electricity and thermal vectors, integrating PV power plant, BESS and electrical loads (in electricity vector) and gas boiler, heat pump, electric boiler and underfloor demand (in thermal vector).
- Development of a dynamic fuzzy logic-based EMS that provides an efficient energy distribution in the MEMG and allows a wide operating range for thermal and electricity vectors.
- Validation of the proposed MEMG and EMS under different weather condition and variations in electric and thermal loads. The results demonstrate significant improvements compared to a conventional state-based EMS, achieving a significant 80% reduction in local grid utilization for the tested scenarios. Furthermore, energy reductions of 7.4% and 5.4% are achieved for the gas and electric boiler sources, respectively.
- Real-time verification using experimental hardware-in-the-loop (HIL) setup for the proposed MEMG. The MEMG operates on an OPAL4512 unit, while the control system is implemented on a dSPACE MicroLabBox prototype. This real-world testing confirms the effectiveness of the proposed EMS under practical operating conditions.

Following this introduction, Section II provides a detailed explanation of the MEMG under study. The proposed control scheme and fuzzy logic-EMS are described in Section III. Section IV introduces an alternative state-based EMS for comparison with the proposed fuzzy-logic EMS. Section V validates the operation of the MEMG under different scenarios using MATLAB/Simulink and presents the experimental results. Finally, Section VI provides the conclusions drawn in this paper.

II. DYNAMIC MODELLING OF THE MEMG

Fig. 1 shows the configuration of the proposed MEMG. The thermal segment of the MEMG comprises a 10-kW gas boiler and a 23-kW electric boiler with a 300-liter storage capacity, catering the heat demand of the MEMG. The electrical vector incorporates an 18-kW PV power plant, consisting of 60 panels of 300 W each. The PV power plant layout is designed using six strings of 10 panels connected in series per string. To mitigate the fluctuations inherent in PV power generation, a Lithium-Ion based BESS is integrated, leveraging its advantages in efficiency and scalability [27]. The selected BESS has a rated capacity of 26.6 kWh and a rated voltage of 345V. Furthermore, the MEMG is connected to a 400 V three-phase local grid to ensure a reliable power supply.

It is important to note that the controlled components in the MEMG are the electric and gas boilers, along with the BESS. The PV power plant operates at the maximum power point tracking (MPPT) to maximize its output, while the local grid assumes the surplus or necessary power to fulfill the demand fluctuations.

The modelling of the MEMG is implemented in MATLAB/Simulink. The CARNOT Toolbox, developed by the Institute of Solar Research in Juelich, Germany, was employed to model the thermal components of MEMG [28]. This toolbox provides a comprehensive library of components commonly used in thermal systems, represented by modular blocksets. Additionally, it offers valuable insights into the coordination between electrical and thermal systems, as well as specific elements related to thermal loads [28].

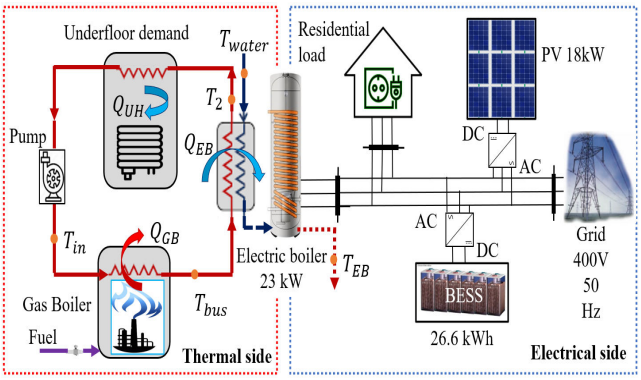

FIGURE 1. Schematic diagram of the electrical-thermal MEMG.

A. THERMAL VECTOR

The aforementioned thermal sources thermal loads form a thermal system that needs a structured and organized operational framework.

Fig. 1 illustrates the thermal system scheme proposed in this paper. A thermal bus, a closed thermal circuit connecting the thermal sources and loads, is employed. A gas boiler maintains the bus temperature $(T_{bus}^{\square})$ at the desired value. The electric boiler extracts heat (denoted as Q_{EB}^{out}) from the bus by warming water obtained from the local network to achieve $T_{bus}^{\square}$.

Subsequently, the electric boiler elevates this temperature to the required hot water demand $(T_{EB}^{\square})$. Finally, an independent heat exchanger connects the underfloor heating demand to the bus, extracting heat power (denoted as $Q_{U.H}^{\square}$) from the bus. This process results in a temperature reduction to $T_{in}^{\square}$, which serves as the input temperature for the gas boiler.

The thermal bus serves as the central component, facilitating heat transfer among the boilers and thermal loads, and control of water temperature. It enables efficient energy utilization and structured system organization by employing hot water circulation within the heating loop.

To account for temperature drops during the heat exchange process, Eqs. (1) and (2) model the heat exchange between the electric boiler and the underfloor heating based on the thermodynamic energy balance principle:

$$T_2 = \frac{\dot{m}_{water} \cdot T_{water} + \dot{m}_{bus} \cdot T_{bus}}{\dot{m}_{water} + \dot{m}_{bus}} \tag{1}$$

$$T_{in} = T_2 + \frac{-Q_{U.H}^{\square}}{\dot{m}_{bus} \cdot c_{p\square}} \tag{2}$$

The gas boiler model is a simplified representation that primarily focuses on the heat input into the boiler combustion chamber. It disregards any limitations arising from the process or combustion control, such as the initial burner control during start-up. For the water side of the boiler, a multinode model is utilized to capture the time-dependent conditions. The differential equation governing the gas boiler is given as [29]:

$$\left(m \cdot c \cdot \frac{1}{N}\right) \cdot \frac{dT_{bus}}{dt} = \left(U \cdot A \cdot \frac{1}{N}\right) \cdot (T_{amb} - T_{bus}) + (\dot{m}_{bus} \cdot c_f) \cdot (T_{in} - T_{bus}) + Q_{GB} \tag{3}$$

To define (3), the law of conservation of energy and the first law of thermodynamics are employed. In this expression, the rate of change of the gas boiler's outlet temperature with respect to time equals the sum of heat transfer with the surroundings due to the heat flow through the boiler ducts (first term), the amount of heat required to raise the water from the inlet temperature to the desired outlet temperature (second term), and the heat supplied by the gas boiler, Q_{GB} (third term).

The electric boiler is modelled as an electric heater, utilizing electricity to heat the incoming mass flow of the water network for domestic hot water consumption. A thermal node represents the thermal inertia of the heater and account for losses to the surrounding environment. The equation governing the electric boiler is described by [28]:

$$mcp \cdot \frac{dT_{EB}}{dt} = U \cdot A \cdot (T_{amb} - T_{EB}) + (\dot{m}_{water} \cdot c_p) \cdot (T_{bus} - T_{EB}) + P_{EB} \tag{4}$$

which was defined using the law of conservation of energy and the first law of thermodynamics. In (4), the rate of change of temperature at the outlet with respect to time, considering the boiler's capacity mcp, is expressed as the losses to the

surroundings due to heat flow through the boiler pipes (first term), the heat required to raise the water temperature from the inlet temperature to the desired outlet temperature (second term), and the required electrical power, P_{EB} (third term).

B. ELECTRICITY VECTOR

The PV system implementation described in [30] is chosen due to its proven accuracy and simplicity [31]. The I-V characteristics of this model are obtained by providing irradiance and temperature as input. The model comprises a diode, a controlled current source, and two resistances (one in series and one in parallel). The mathematical expression for the output current of the PV system is as follows:

$$I_{PV} = I_L - I_{sat}\left(e^{\frac{q(V_{PV}+I_{PV}R_S)}{N_S K T_{PV}}}\right) - (V_{PV} + I_{PV}R_S)/\,R_{sh} \quad (5)$$

$$I_L = L_{L0}(1 + K_0(T_{PV} - 300)\frac{G_s}{G_n} \quad (6)$$

$$I_{sat} = K_1 T_{PV}^3 e^{-qV_g/T_{PV}} \quad (7)$$

This paper employs a BESS model derived from the SimPowerSystems Toolbox of Simulink [32]. To ensure accuracy, modifications have been made to accurately depict the V-I and V-SOC curves, as well as the dynamic response of the battery, based in datasheets information. The model consists of a series resistance and a variable voltage source.

$$V_{BESS} = E_{BESS} - I_{BESS} \cdot R_{int} \quad (8)$$

Additionally, the battery state-of-charge (SOC), which is calculated from the BESS current variation, is a critical parameter that requires a suitable control to prevent overcharging or deep discharging.

III. FUZZY LOGIC-BASED DYNAMIC EMS AND CONTROL LOOPS

This section introduces the novel fuzzy logic-based dynamic EMS and the control loops proposed for the MEMG described in Section II. The primary objective of the EMS is to maintain power balance (electrical and thermal) by coordinating the operation of the gas and electric boilers alongside the production of the PV power plant, BESS, and thermal and electrical loads, while minimizing the utilization of the local grid.

This goal allows the MEMG to operate as an independent MG, while the control loops ensure the local control of each component. In this context, the electric boiler control loop regulates T_{EB} following a hysteresis cycle. The gas boiler control loop is implemented using a PI controller, which regulates T_{bus}. Additionally, the MPPT strategy based on P& O algorithm is implemented for the PV power plant, and the BESS is controlled according to its SOC. The EMS acts as a supervisory control for the entire MEMG.

A. FUZZY LOGIC-BASED DYNAMIC EMS

The proposed FL-based dynamic EMS relies on taking into account the renewable available power (P_{PV}), the electric load and the BESS SOC to determinate dynamically the operating point of the thermal components of the MEMG, which involves varying T_{EB}, P_{EB} T_{bus} and Q_{GB}, while satisfying both electrical and thermal demands. Besides, the fuzzy logic system ensures power balance (both electrical and thermal) and minimizes the utilization of the local grid.

By employing fuzzy logic, the boiler can operate over a wide temperature range generating both the turn-on (T_{EB}^{min}) and turn-off (T_{EB}^{max}) temperatures in the electric boiler. The reference bus temperature can also be adjusted depending on the MEMG needs.

The novelty in the proposed FL-EMS lies in its structure and its objective to coordinate the operation of electrical and thermal components. It is based on knowing the available energy in the MEMG at each moment. For this purpose, it only needs two parameters: the gross net power (P'_{NET}) and the BESS SOC. It provides the output signals T_{EB}^{max}, P_{EB} and T_{bus}, which allow understanding the energy consumption of the electric and gas boilers.

The designed FL controller considers two inputs and three outputs, as shown in Fig. 2. In MGs, the difference between renewable power and demanded load is typically defined as $P_{NET}^{\square}$. For the EMS presented in this paper, the demanded load is divided into the electrical load (power demanded by the dwelling) and the power demanded by the electric boiler. In addition, P'_{NET} is defined as $P_{NET}^{\square}$ without considering the electric boiler demand (P_{EB}):

$$P'_{NET} = P_{PV} - P_{LOAD} \quad (9)$$

$$P_{NET}^{\square} = P_{PV} - (P_{LOAD} + P_{EB}) \quad (10)$$

Note that the BESS power (P_{BESS}) can be calculated as the difference between P'_{NET}-P_{EB} and is limited by its current SOC, as described in Eqs. (11) and (12) and illustrated in Fig. 2.

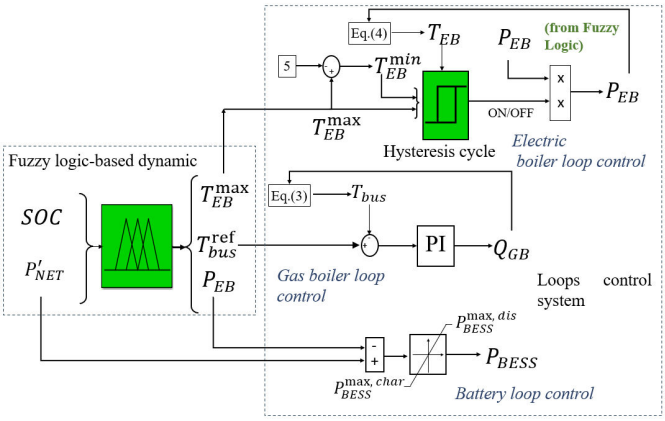

Fig. 2. Overall MEMG scheme control.

$$P_{BESS,dis}^{max} = min\left(P_{BESS}^{max}, \frac{E_{BESS}^{nom}}{\Delta t} \cdot \left(\frac{SOC - SOC_{min}}{100}\right)\right) \quad (11)$$

$$P_{BESS,ch}^{max} = min\left(P_{BESS}^{max}, \frac{E_{BESS}^{nom}}{\Delta t} \cdot \left(\frac{SOC_{max} - SOC}{100}\right)\right) \quad (12)$$

P_{BESS} constraints shown in Eqs. (11) and (12) determine the maximum power that the BESS can handle (P_{BESS}^{max}). On the one hand, P_{BES}^{max} is limited according to the rated power of the BESS. In addition, the SOC restriction guarantees that the maximum power available is limited according to the SOC in each moment without exceeding a threshold value.

This restriction is based on maintaining the SOC level within a safe operating zone, defined by upper and lower limits (SOC_{max}, SOC_{min}). The upper limit is set at 90 % and the lower limit to 30%. The BESS cannot be discharged below SOC_{min} or charged above SOC_{max}.

Furthermore, in discharging mode, the maximum power delivered by the BESS is proportional to the SOC level when the SOC is between 30% and 50%.

The design of the FL-EMS consists of three stages, namely: fuzzification, rule-base, and defuzzification. The fuzzification module transforms physical values into a normalized fuzzy subset, consisting of an interval for the range of input values, and an associated membership function describing the confidence levels that the input belongs to this range. The purpose of this step is to make the physical input signal compatible with the fuzzy control rule base at the core of the controller.

Five membership functions (MFs) are utilized for fuzzification to define P'_{NET}: negative high (NH), negative (N), zero (Z), positive (P) and positive high (PH). Three MFs are employed for SOC, P_{EB} and T_{max}^{EB}: low (L), normal (N) and high (H). T_{GB} is defined with two MFs: low (L) and high (H).

The rule base process is crucial for achieving the ultimate goal of minimizing energy consumption. It focuses on determining the operating mode of the output variables based on the input variables.

The MF distribution is shown in Fig. 3. In this study, 15 rules (see Table I) are used to determine the system behavior using a Mamdani-type inference method. This method was chosen due to its ease of implementation and its ability to handle nonlinear systems. Its flexibility and adaptability to new data or system changes make it suitable for dynamic scenarios, as is the case investigated in this study [33].

Serving as an intermediary between the control rule base and the physical system under control, the defuzzification module acts as a bridge, converting the controller outputs (produced by the control rule base in fuzzy terms) into precise values that the system can handle. In this article, the centroid method is employed as the defuzzification technique.

$$u\big((k+1)T\big) = \frac{\sum_{i=1}^{N} \mu_{U_i}\big(u_i(kT)\big) \cdot u_i(kT)}{\sum_{i=1}^{N} \mu_{U_i}\big(u_i(kT)\big)} \quad (13)$$

Here, T represents the sampling time, and $u(kT)$ denotes the value of the new control action change, u_i refers to the fuzzy subsets comprising bounded intervals with their associated membership functions, and μU denotes the weights for centroid defuzzification.

Fuzzy logic enables a flexible consumption pattern by dynamically adjusting P_{EB} based on P'_{NET} and SOC, rather than keeping it constant its rated power. For instance, when P'_{NET} is positive and SOC is high, the electric boiler operates as the primary heat source, and the BESS charges accordingly. Conversely, if P'_{NET} is negative and SOC is low, the available P_{EB} decreases, restricting the BESS from discharging.

A similar approach is employed for bus thermal temperature control, where T_{bus} varies across a range of temperatures, providing multiple operating points. This control structure

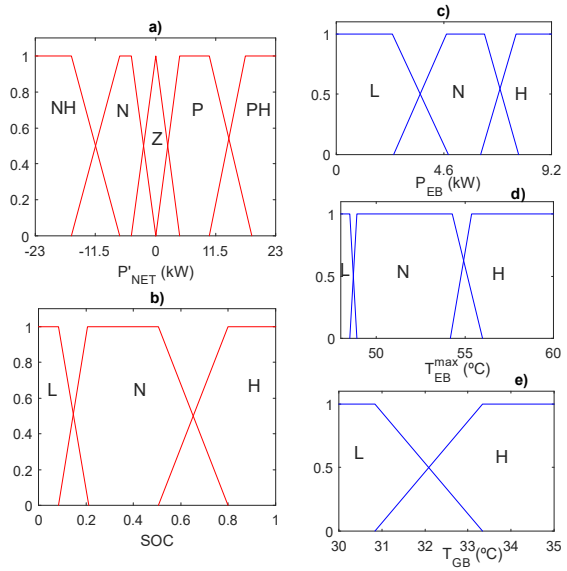

Fig. 3. Membership functions: a) Gross net power (P'_{NET}), b) BES SOC, c) electric boiler power (P_{EB}), d) electric boiler turn-off temperature (T_{max}^{EB}), and e) temperature in the thermal bus (T_{bus}).

TABLE I
RULE BASE OF THE FUZZY LOGIC EMS

		P'_{NET}														
		NH			N			Z			P			PH		
		P_{EB}^{pu}	T_{EB}^{max}	T_{bus}	P_{EB}^{pu}	T_{EB}^{max}	T_{bus}	P_{EB}^{pu}	T_{EB}^{max}	T_{bus}	P_{EB}^{pu}	T_{EB}^{max}	T_{bus}	P_{EB}^{pu}	T_{EB}^{max}	T_{bus}
SOC	L	Z	L	H	Z	L	H	Z	N	H	N	N	H	H	N	H
	N	Z	L	H	N	N	H	N	N	H	N	N	H	H	H	L
	H	N	N	H	N	H	L	H	H	L	H	H	L	H	H	L

promotes intelligent energy usage and reduces energy consumption, as discussed in Section IV.

Designing an EMS requires a deep understanding of the overall system. Inefficient design can lead to complex EMS structures. Previous studies using FL for the EMS of a MEMG often require complex structures. For instance, 14 input parameters and 45 rules was used in [34], 27 inference rules and 3 input variables with 3 membership functions each in [35], and 3 membership functions for each of the 5 selected input variables in [36], resulting in a total of 243 rules.

In contrast, this article proposes a simplified and easily reproducible structure for other MEMG architectures. It utilizes only two input variables: net power P'_{NET} (with 5 membership functions) and SOC (with 3 membership functions). This results in a significantly reduced set of 15 inference rules for optimal FL operation, making it adaptable to MEMG designs with similar characteristics.

B. CONTROL LOOPS

Fig. 2 shows the proposed control loops for the critical components of the MEMG. During the heating process, hot water flow and underfloor heating often fluctuate. The thermal bus control subsystem is responsible for maintaining T_{bus} at the desired reference value (T_{bus}^{ref}).

This is achieved by using a gas boiler to increase the temperature of the incoming water and managing the bus according to the demand for underfloor heating and hot water usage. To accomplish this, a PI controller is employed to regulate Q_{EB} and achieve the target bus temperature. This approach allows the power delivered by the gas boiler to be adjusted to meet the temperature requirements rather than operating in an all-or-nothing operation.

The electric boiler temperature control subsystem regulates the output temperature of the electric boiler (T_{EB}), based on T_{EB}^{max} provided by the EMS. Effective temperature regulation is achieved through the implementation of a hysteresis control cycle.

In this process, the EMS determines the maximum temperature mode for the electric boiler (T_{EB}^{max}) and the minimum temperature mode for the hysteresis cycle (T_{EB}^{min}) is set at 5°C lower than T_{max}^{EB}. As a result, the electric boiler is activated until it reaches the upper threshold, and then it is deactivated until it reaches the lower threshold. This approach ensures temperature control without requiring a constant power supply to the boiler.

The MPPT strategy employs the PV voltage (V_{PV}) and PV current (I_{PV}) to calculate the maximum power point voltage (V_{PV}^{*}) for each operating condition. To achieve this, the Perturb & Observe (P&O) algorithm is selected to perform the MPPT.

This strategy operates by changing the PV voltage and analyzing the output power. Based on these observations, the P&O technique calculates the necessary adjustment direction to approach the maximum power point (MPP).

IV. RESULTS AND DISCUSSION

This section evaluates the performance of the MEMG proposed in Section II, including the fuzzy logic-based dynamic EMS and control loops presented in Section III. MEMG modelling and simulations were performed using MATLAB/Simulink.

The analysis is structured into three sections. First, Section IV.A focuses on the performance of the fuzzy logic-based dynamic EMS. The thermal control of the MEMG is discussed, considering the performance of both the thermal and electrical components of the MEMG.

To illustrate the advantages of the designed fuzzy-logic supervisory control, the results are compared with a flowchart control in Section IV.B. Finally, Section IV.C presents a hardware-in-the-loop experimental setup to validate the MATLAB/Simulink simulations. In this experimental setup, the power system is implemented on an OPAL-RT4512 unit, while the proposed control systems are executed on a dSPACE MicroLabBox unit. The results are then displayed on a Yokogawa DLM4038 oscilloscope, where the signals are scaled down and measured in real time according to the references sent by the dSPACE controller board.

A. EVALUATION OF THE DYNAMIC FUZZY LOGIC-BASED EMS

To ensure a proper response of the dynamic behavior of the MEMG, it is tested over a varying profile of climatic conditions, water consumption, underfloor heating demand and domestic electrical loads over a four-hour simulation.

Fig. 4 shows the profile data for water consumption ($\dot{m}_{water}$), irradiance of the PV power plant, and underfloor heating demand (Q_{UH}).

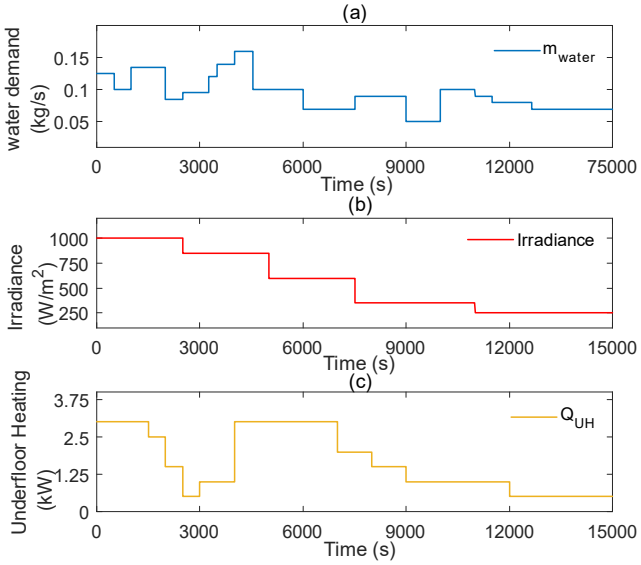

Fig. 4. MEMG operating parameters.

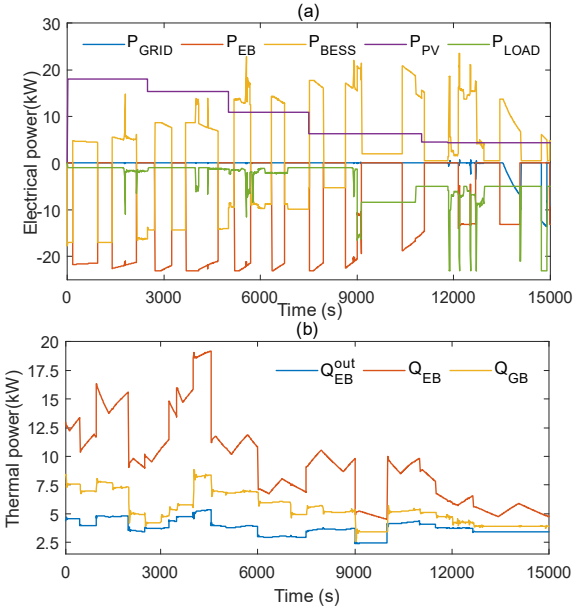

Fig. 5. Balanced power for fuzzy logic-based dynamic EMS: (a) Electric powers and (b) thermal powers.

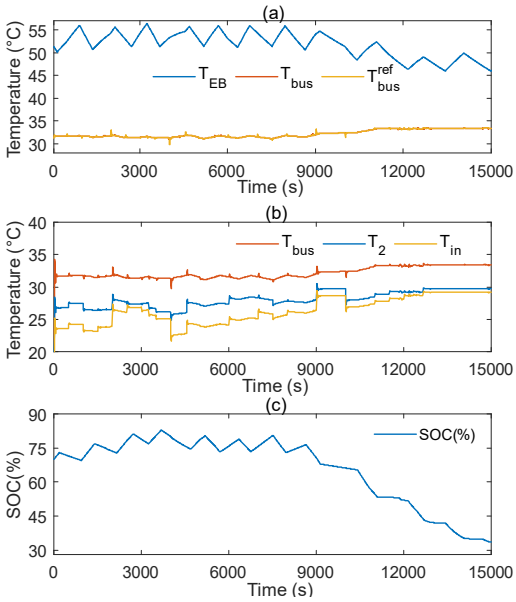

Fig. 6. (a) Electric boiler temperature for fuzzy logic ($T_{EB}^{\square}$), Bus temperature control for fuzzy logic, ($T_{bus}^{\square}$and T_{bus}^{ref}), (b)Temperature drops for fuzzy logic ($T_{bus}^{\square}$, $T_{2}^{\square}$, $T_{in}^{\square}$) and (c) BESS SOC for fuzzy logic-based dynamic EMS.

Fig. 5 shows the electrical and thermal powers of the MEMG. The power balance for electrical powers is illustrated in Fig. 5a. Between 0 to 2500s, the PV power plant produces 17.95 kW, while the electric boiler consumes 21.5 kW when it is turned on. When the electric boiler reaches the upper temperature setpoint determined by the hysteresis control, it is turned off. In this situation, the BESS is charged at a higher value of 16.95 kW.

When the electric load demand ($P_{LOAD}^{\square}$) increases, P'_{NET} decreases, and consequently, $P_{EB}^{\square}$ decreases in accordance with the reference signal generated by the fuzzy logic-based dynamic EMS.

At 7500s, the PV production drops to 6.3 kW. This operating condition implies that as $P_{LOAD}^{\square}$ increases, the BESS changes to discharging mode while $P_{EB}^{\square}$ reduces due to lower renewable power availability. The BESS remains in discharging mode, and when the SOC is near to the minimum SOC level ($SOC_{min}^{\square} = 30\%$), the BESS is not able to fulfill the demands, and the local grid must provide the necessary power to the MEMG. The fuzzy logic-based dynamic EMS, upon receiving signals indicating a lower SOC and lower $P_{PV}^{\square}$, sets a minimum value for $P_{EB}^{\square}$.

The thermal power balance is illustrated in Fig. 5b. It shows the heat extracted from the bus due to hot water consumption in the fuzzy logic control (Q_{EB}^{out}), the heat injected by the electric boiler in the fuzzy logic control ($Q_{EB}^{\square}$), and the heat provided by the gas boiler $\left(Q_{GB}^{\square}\right)$.

As seen, when there is an increment in $\dot{m}_{water}$ or $Q_{UH}^{\square}$, $Q_{EB}^{\square}$ increases its value. Consequently, $Q_{GB}^{\square}$ is incremented to maintain the bus temperature at the required value.

As discussed in Section III, the gas boiler is responsible for maintaining the temperature of the thermal bus, while the electric boiler increases the temperature to fulfill the domestic hot water demand. Fig. 6a shows the measured electric boiler output temperature for the fuzzy logic control $\left(T_{EB}^{\square}\right)$, which varies according to the operation point of the MEMG at each moment.

This figure also includes the measured temperature control of the gas boiler for the fuzzy logic control ($T_{bus}^{\square}$) and the reference temperature control (T_{bus}^{ref}). Heat exchangers connect the different thermal components, and $T_{bus}^{\square}$ decreases due to the heat extracted from the bus.

Furthermore, Fig. 6b represents the output temperature of the gas boiler ($T_{bus}^{\square}$), the temperature after the heat exchanged with the electric boiler ($T_{2}^{\square}$), and the temperature after the heat exchange with the underfloor heating, which coincides with the input temperature of the gas boiler ($T_{in}^{\square}$).

The BESS SOC control is represented in Fig. 6c. The SOC is maintained between $SOC_{min}^{\square}$ and $SOC_{max}^{\square}$. When the SOC approaches $SOC_{min}^{\square}$, the curve becomes less decreasing for the discharging, aligning with the goal of not exceeding $SOC_{min}^{\square}$.

B. EVALUATION OF THE STATES-BASED EMS

To compare the fuzzy logic-based dynamic EMS discussed in Section III, this section outlines an alternative EMS known as states-based EMS, which is based on operating states. Fig. 7 represents the flowchart of this EMS. It generates the same variables as the fuzzy logic-based dynamic EMS, i.e, to obtain T_{max}^{EB}, P_{EB} and T_{bus}, pursuing the same targets.
Similarly, the input signals are P'_{NET}, P_{EB}, and the maximum power available in the BESS ($P_{BESS}^{\max}$). The outputs are the operating modes for the gas and the electric boilers, and P_{BESS} is calculated according to Eqs (11,12).

On the basis of these definitions, the following five possible modes of operation are defined:

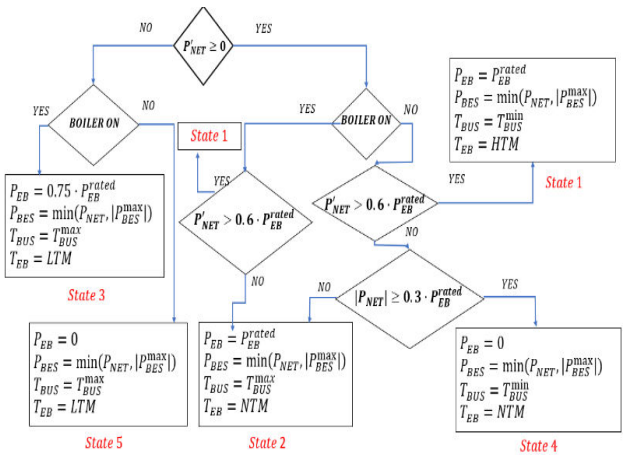

Fig. 7. Flowchart states-based EMS.

- High-temperature mode (HTM): When $P'_{NET} > 0$ and $P'_{NET} > 0.6 \cdot P_{EB}^{rated}$, the system operates with excess renewable power. In this mode, the electric boiler is turned on, while the gas boiler operates at a lower temperature. The excess renewable power is managed by the BESS, which charges according to its SOC. Moreover, if the electric boiler is turned off and $P'_{NET} > 0.6 \cdot P_{EB}^{rated}$, the EMS sends the order to turn on the electric boiler in this operation mode.
- Normal-temperature mode (NTM): In the case of $P'_{NET} > 0$, and $P'_{NET} < 0.6 \cdot P_{EB}^{rated}$, the electric boiler operates in NTM, and the gas boiler increases its temperature. The BESS discharges to meet the electric demand. When $P'_{NET} < 0.6 \cdot P_{EB}^{rated}$ and $|P_{NET}^{\square}| < 0.3 \cdot P_{EB}^{rated}$, the boiler is turned on.
- Low-temperature mode (LTM): If $P'_{NET} < 0$, the electric boiler is activated at low temperatures, while the gas boiler increases its temperature similarly to NTM. If the boiler is turned off, it remains in the LTM.
- Off mode (NTM): When $P'_{NET} > 0$, and $P'_{NET} < P_{EB}^{rated}$, if $|P_{NET}^{\square}| > 0.3 \cdot P_{EB}^{rated}$, the boiler remains turned off in NTM.
- Off mode (LTM): When $P'_{NET} < 0$ and the boiler is turned off, it remains turned off in LTM.

The results for the states-based EMS are shown in Fig. 8, which are denoted as "ST". The electric powers are represented in Fig. 8a. As mentioned above, the MEMG operation is divided into HTM, NTM, and LTM. From 0 to 6000s, the MEMG operates in alternating HTM and NTM modes. The electric boiler consumes its rated power, which is 23 kW, and the BESS is less charged than in Fig. 5a.

In contrast, when $P_{LOAD}^{\square}$ increases, $P_{EB}^{\square}$ is kept at rated power, and the MEMG operates in MTM. This implies that the BESS is further discharged to fulfill the demand. Therefore, in this situation, the BESS handles the peaks value of the domestic electrical loads and $P_{EB}^{\square}$. From 12000s onward, the MEMG operates in LTM and $P_{EB}^{\square}$ is decreased. Similarly, when the SOC is near to $SOC_{min}^{\square}$, the local grid injects the required power to the MEMG as there is not renewable or storage system energy available.

Analogously, the thermal powers are shown in Fig. 8.b, where the same parameters are represented for the states-based EMS: $Q_{E.B}^{out-ST}$, $Q_{E.B}^{ST}$ and $Q_{G.B}^{ST}$, respectively. As shown, a minor amount of heat power is required for the fuzzy-logic control to maintain the temperature, leading to a lower electrical energy consumption of the electric boiler, as shown in Table II.

On the other hand, Fig. 8c shows the temperature of the electric boiler for the states-based EMS (T_{EB}^{ST}). In this case, T_{EB}^{ST} is controlled in HTM and MTM from 0 to 6000s, in MTM from 6000s to 10500s and in LTM from 10500s to 15000s. Moreover, Fig. 8c represents the measured temperature control of the gas boiler for the states-based EMS (T_{bus}^{ST}) and the reference temperature control (T_{bus}^{ref-ST}).

In this instance, T_{bus}^{ST} takes a value of 30 °C if the electric boiler operates in HTM and a value of 35 °C if the electric boiler operates in MTM or LTM. The temperature drops due to the heat exchanged in the thermal bus are represented in Fig. 8d for the states-based EMS, which are denoted as T_{bus}^{ST}, , T_2^{ST} and T_{in}^{ST}.

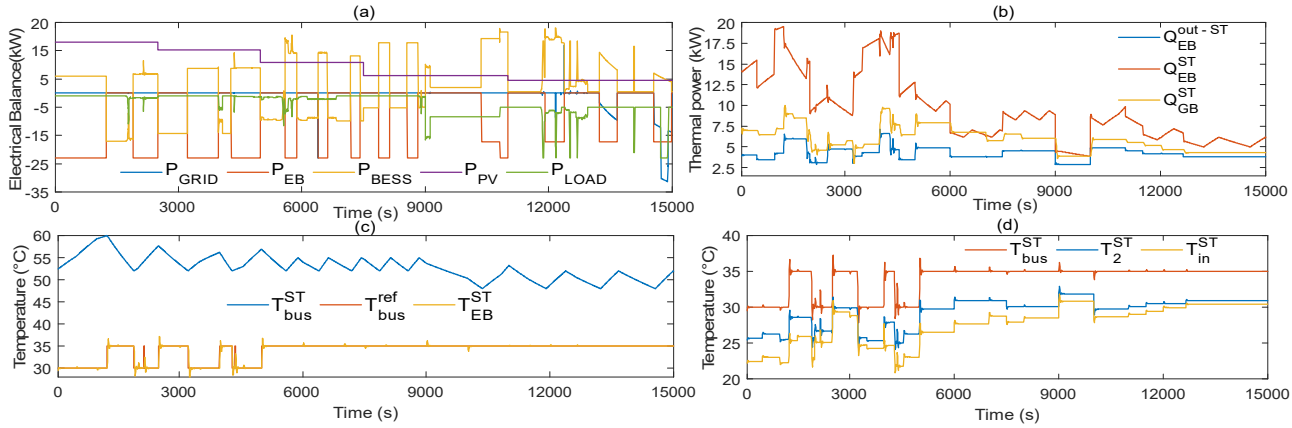

Fig. 8. States-bases EMS (a) Electric powers and (b) thermal powers, (c) Electric boiler temperature T_{EB}^{ST}, Bus temperature control ($T_{bus}^{ST}$and T_{bus}^{ref}) and (d) Temperature drops ($T_{bus}^{ST}, T_2^{ST}, T_{in}^{ST}$).

Finally, to ensure the correct operation of the MEMG, the energy balance in the thermal bus must be satisfied. This means that the total heat extracted from the bus (Q_{con}), which is the sum of the underfloor heating demand ($Q_{U.H}$), and the heat extracted for the electric boiler ($Q_{E.B}^{out}$), must be equal to the heat injected by the gas boiler ($Q_{G.B}$) to maintain T_{bus} according to T_{bus}^{ref}.

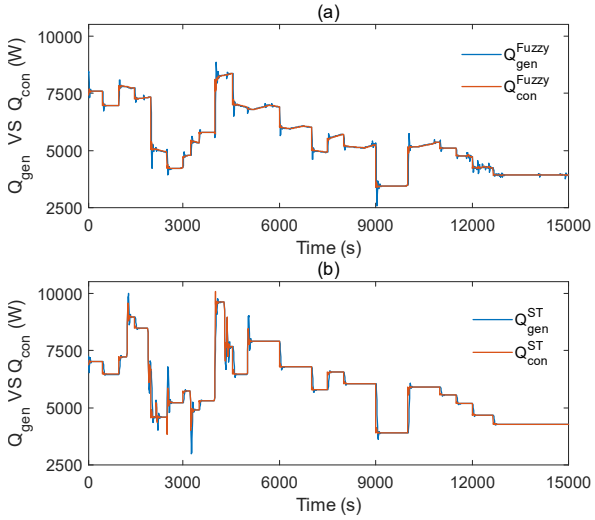

Fig. 9. (a) Thermal energy balance for fuzzy logic-based dynamic EMS and (b) electric power balance for state-based EMS.

Fig. 9a shows the energy balance for the fuzzy logic control, while Fig. 9b represents the same concept for the states-based control, where adequate responses are achieved in both cases. To provide numerical support to the above discussion, it has been calculated how the electric boiler power is supplied. The total energy consumed by the gas boiler can be computed by integrating the supplied power. Table II illustrates the total energy consumed (E_{GB}) for the fuzzy-based EMS and the states-based EMS. The results demonstrate a 7.36% reduction in consumption for the presented fuzzy-based EMS.

Furthermore, Table II presents the energy consumed by the electric and gas boiler. As seen, the energy demand of the electric boiler (E_{EB}) is reduced by 5.38 % for the fuzzy-based EMS. The total consumption of the local grid (E_{grid}) is notably reduced by 80.67% for the fuzzy-based EMS, highlighting its superiority over the states-based EMS. The savings lie in the fact that the proposed fuzzy-based EMS is able to dynamically adjust the operating point of the electric and gas boilers, while the state-based EMS maintains a fixed consumption pattern for each operating mode. This dynamic adaptation enables more efficient energy distribution, resulting in energy savings as demonstrated by the numerical analysis.

Another interesting aspect to analyze is the technology employed to supply the electric boiler. In terms of utilization, the fuzzy EMS enables a 1.74% increase in renewable power utilization (G_{PV}), and a 4.93% rise in BESS power utilization G_{BESS}). This results in a 6.67% decrease in grid utilization (G_{GRID}) when compared to states-based EMS. Consequently, the grid is also less employed to fulfill the demand in each case, demonstrating the superiority of the proposed fuzzy EMS.

It is essential to note that despite the different control schemes used, the average temperatures for the electric boiler (T_{EB}^{avg}), and the gas boiler (T_{GB}^{avg}) are very similar in both cases, ensuring consistent thermal comfort, as demonstrated in Table II.

TABLE II
NUMERICAL COMPARISON BETWEEN FUZZY LOGIC-BASED DYNAMIC EMS AND STATES-BASED EMS

Variable	Fuzzy-based EMS	States-based EMS	% Variation	% Utilization	
				Fuzzy EMS	States EMS
T_{EB}(°C)	52.22	52.83	1.15	-	-
T_{bus}^{avg}(°C)	32.76	33.89	3.33	-	-
E_{GRID}(kWh)	0.63	3.26	-80.67	-	-
E_{GB}(kWh)	22.66	24.46	-7.36	-	-
E_{EB}(kWh)	37.11	39.22	-5.38	-	-
G_{PV}(kWh)	15.21	15.40	1.74	41.00	39.26
G_{BESS}(kWh)	21.27	20.55	4.93	57.32	52.39
G_{GRID}(kWh)	0.63	3.26	-6.67	1.69	8.31
Total gen. (kWh)	37.11	39.22	-	-	-

In addition to an energy-based comparison, this section presents the metrics used to quantitatively evaluate the control performance of the FL-EMS compared against the SB-EMS, as well as the BESS SOC behavior and the temperature gradient in the gas boiler. Table III summarized the numerical results.

Firstly, performance indices including the Integral Time Absolute Error (ITAE), Integral Time Squared Error ITSE), Integral Absolute Error (IAE), and Integral Squared Error (ISE) are computed for of the regulated T_{bus} with respect to its reference, T_{bus}^{ref}, and for the regulated Q_{GEN} with respect to Q_{CON}. The results show an improvement in $ITAE_{Tbus}$ of 42.57%, in $ITSE_{Tbus}$ of 89.1%, IAE_{Tbus} of 54.36%, and in ISE_{Tbus} of 57.55%. Regarding the thermal balance control, the improvement in $ITAE_{Q}$ is 17.06%, in $ITSE_{Q}$ is 52.5%, in IAE_{Q} is 31.19%, and in ISE_{Q} is 29.99%.

Employing FL-EMS results in an increase of 5.03% in the maximum BESS SOC (SOC_{max}), 1.6% in the minimum BESS SOC (SOC_{min}), and 3.98% in the average BESS SOC (SOC_{avg}). This demonstrates that the BESS is managed more effectively with the proposed FL-EMS.

Finally, the temperature gradient in the gas boiler is calculated, which is defined as $\Delta T = (T_{bus} - T_{in})$. The parameter ΔT is directly related to the heat that the gas boiler must generate to meet the thermal demand. The results show

TABLE III
METRICS FOR EVALUATE THE FUZZY LOGIC-BASED DYNAMIC EMS AND STATES-BASED EMS

Variable	Fuzzy-based EMS	States-based EMS	% Variation
ITAE T_{bus}	$2.516 \cdot 10^6$	$4.381 \cdot 10^6$	-42.57%
ITSE T_{bus}	$8.687 \cdot 10^6$	$7.971 \cdot 10^7$	-89.10%
IAE T_{bus}	587.4	1287	-54.36%
ISE T_{bus}	1391	3277	-57.55%
ITAE Q	$3.976 \cdot 10^9$	$4.794 \cdot 10^9$	-17.06%
ITSE Q	$1.919 \cdot 10^{12}$	$1.919 \cdot 10^{12}$	-52.50%
IAE Q	$8.587 \cdot 10^5$	$1.248 \cdot 10^6$	-31.19%
ISE Q	$1.716 \cdot 10^9$	$2.451 \cdot 10^9$	-29.99%
SOC_{max} (%)	82.89	78.92	5.03%
SOC_{min} (%)	33.57	33.04	1.60%
SOC_{avg}(%)	65.88	63.36	3.98%
ΔT_{in} (ºC)	5.85	6.21	-7.29%

a decrease in the temperature gradient for the FL-EMS of 7.29%.

C. HARDWARE-IN-THE-LOOP (HIL) VERIFICATION

Fig. 10a shows the schematic of the experimental setup built in the laboratory to perform a real-time simulation based on the HIL. The power system is implemented using an OPAL-RT4512 unit, a real-time HIL simulator designed for executing and testing models created using MATLAB/Simulink.

It is specifically programmed using RT-Lab software, enabling efficient model implementation and testing. The control system is executed on a DSPACE MicroLabBox unit, programmed using Simulink. DSPACE MicroLabBox is a hardware device dedicated to rapid control prototyping and algorithm testing.

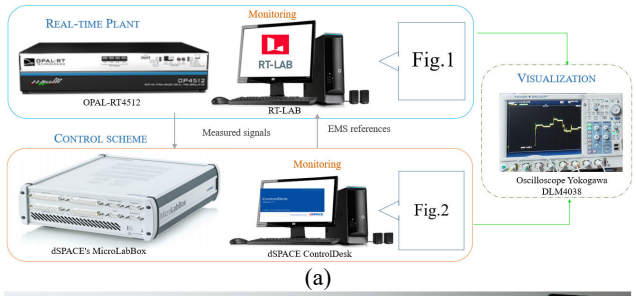

(a)

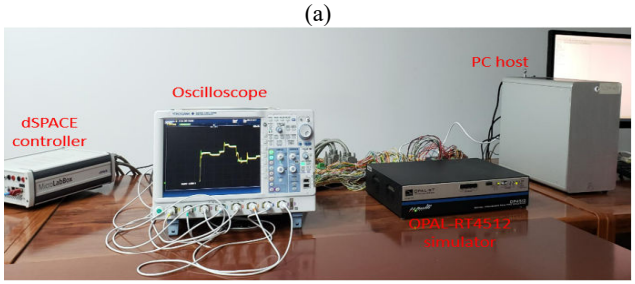

(b)

Fig. 10. Experimental HIL setup implemented in the laboratory:(a) Scheme, (b) Photo.

It incorporates a powerful FPGA, and a comprehensive suite of I/O interfaces. Real-time simulation visualization is achieved using a Yokogawa DLM4038 oscilloscope. The Yokogawa DLM4038 is a digital storage oscilloscope specifically designed for accurate waveform analysis. Fig. 10b illustrates the experimental setup.

It is worth noting that the OPAL-RT4512 analogue outputs operate within the range of -16V/+16V. Consequently, signals measured in the MATLAB/Simulink simulation must be scaled down to ensure proper representation on the oscilloscope.

Fig. 11a represents the electric power balance for fuzzy-based dynamic EMS during a 3000s real-time simulation. Initially, the signals were scaled down by dividing them by 2000. Subsequently, a scale of 5V/div was employed to visualize the signals, and a scale of 300 s/div was selected as the time scale.

For instance, the P_{PV} signal (blue) exhibits a value of 17.95 kW in the first stage of the simulation, as seen in Fig. 5a. When divided by 2000 and represented in a scale of 5V/div, the measured signal is approximately 9 V, consistent with the performed scaling.

A similar procedure was applied to the remaining signals: P_{GRID} (yellow), P_{EB} (green), P_{BESS} (purple), and P_{LOAD} (red).

(a)

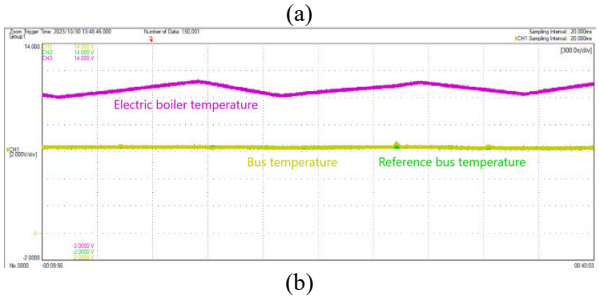

(b)

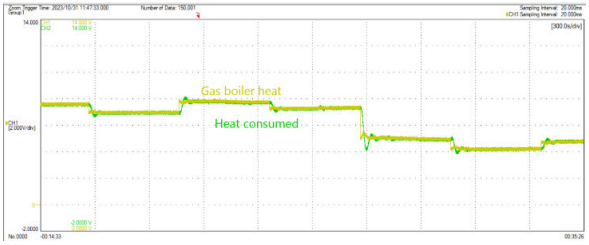

(c)

Fig. 11. Experimental results: (a) Electric power balance, (b) Temperature control and (c) Thermal power balance.

The obtained results confirmed that no energy was consumed from the grid and verified the results obtained from MATLAB/Simulink, as shown Fig. 5a.

Fig. 11b shows the temperature control for fuzzy-based dynamic EMS. In this case, the signals were scaled down by dividing them by 2000. A scale of 2V/div is employed to represent the signals, and the scale of 300 s/div is kept. T_{bus} (yellow) exhibits a value of 32ºC in the first stage of simulation (Fig. 6a). When divided by 5 and represented on a scale of 2V/div, the measured signal is 6.4 V, confirming accurate representation. The same scaling procedure was applied to T_{bus}^{ref} (green) and T_{EB} (purple). It was verified that T_{bus} is controlled according to T_{bus}^{ref}, and the measured results for T_{EB} are consistent with the simulated results (Fig. 6a).

Finally, Fig. 11c illustrates the heat bus control for fuzzy-based dynamic EMS. The signals were scaled down by dividing them by 1000. A scale of 2V/div was used to represent the signals, and the scale of 300 s/div was maintained.

For instance, Q_{GB} (yellow) takes a value of 7.5 kW at the beginning of the simulation (Fig. 9a), and when divided by 1000 and represented in a scale of 2V/div, the measured signal is 7.5 V, further confirming correct representation. The experimental results corroborate the heat control in the thermal bus. The results obtained in the HIL-based real-time simulation have verified the correct performance of the proposed MEMG.

The results validate the effectiveness of both the dynamic models and the proposed novel FL-EMS for MEMGs. The FL-EMS demonstrated significant improvements in terms of energy efficiency and dynamic control of MEMGs. This work could be extended by considering the optimal operational costs in the energy distribution, and exploring demand response services to enhance the operational flexibility of MEMGs.

V. CONCLUSION

Traditionally, MEMG studies have employed a static approach, with optimization algorithms operating over daily or weekly time horizons. These models, typically linearized around a single operating point, may become ineffective when operating conditions deviate. The dynamic study of MEMGs, encompassing real-time control and management systems, which could be improved by the adoption of intelligent control algorithms specifically designed for MEMGs.

This paper provided a dynamic control for a MEMG with electricity and thermal vectors, encompassing generation, energy storage and load systems. To effectively coordinate the different energy vectors within the MEMG, a dynamic fuzzy-based EMS was proposed. The validity of the proposed EMS was evaluated through real-time HIL experimentation.

Minimizing energy consumption through real-time interconnection of diverse energy vectors represents an underexplored approach for optimizing the operation of MEMGs.

The proposed EMS was comparatively evaluated with a state-based EMS. By dynamically adjusting the operating point of the thermal generation sources based on available renewable energy, the proposed fuzzy-based EMS achieved a significant reduction of 80% in power grid consumption, accompanied by a decrease of 7.4% in gas boiler consumption, and a reduction of 5.4% in electric boiler consumption. Additionally, compared to the states-based EMS, the use of the PV plant increased by 1.74%, while BESS utilization rose by 4.93% to feed the electric boiler.

The control of dispatchable and non-dispatchable systems within the context of MEMGs is a sparsely addressed issue in the literature. Concerning the control system, an 89.10% improvement in ITSE was achieved when compared to the states-based EMS for controlling the temperature of the hot water circuit, and a 52.5% improvement in ITSE was achieved for thermal balance control. Additionally, the average SOC was 3.98% higher, and the required temperature jump in the gas boiler was reduced by 7.29%.

Despite the differences in energy dispatch between the two EMS implementations investigated in this paper, the findings demonstrated that thermal comfort was maintained when either a gas or an electric boiler was adopted, while the BESS SOC was effectively controlled within safe operating thresholds. The comprehensive approach presented in this paper ensures the efficient operation of the different vectors within an MEMG, leading to significant savings in natural gas consumption and overall energy consumption from the local electricity grid, while complying meeting energy demand.

REFERENCES

[1] M. Tostado-Véliz, P. Arévalo, and F. Jurado, "A comprehensive electrical-gas-hydrogen Microgrid model for energy management applications," Energy Convers Manag, vol. 228, no. Nov. 2020, 2021.

[2] Y. G. Son, B. C. Oh, M. A. Acquah, R. Fan, D. M. Kim, and S. Y. Kim, "Multi Energy System with an Associated Energy Hub: A Review," IEEE Access, vol. 9. Institute of Electrical and Electronics Engineers Inc., pp. 127753–127766, 2021. doi: 10.1109/ACCESS.2021.3108142.

[3] E. Guelpa, A. Bischi, V. Verda, M. Chertkov, and H. Lund, "Towards future infrastructures for sustainable multi-energy systems: A review," Energy, vol. 184, pp. 2–21, 2019.

[4] P. Wang, Y. Cao, and Z. Ding, "Flexible Multi-Energy Scheduling Scheme for Data Center to Facilitate Wind Power Integration," IEEE Access, vol. 8, pp. 88876–88891, 2020, doi: 10.1109/ACCESS.2020.2990454.

[5] Multi- Y. Wang, B. Wang, and H. Farjam, "Multi-objective scheduling and optimization for smart energy systems with energy hubs and microgrids," Engineering Science and Technology, an International Journal, vol. 51, Mar. 2024, doi: 10.1016/j.jestch.2024.101649.

[6] G. Comodi, A. Bartolini, F. Carducci, B. Nagaranjan, and A. Romagnoli, "Achieving low carbon local energy communities in hot climates by exploiting networks synergies in multi energy systems," Appl Energy, vol. 256, no. August, p. 113901, 2019.

[7] J. Zhong et al., "Optimal Operation of Energy Hub: An Integrated Model Combined Distributionally Robust Optimization Method with Stackelberg Game," IEEE Trans Sustain Energy, vol. 14, no. 3, 2023, doi: 10.1109/TSTE.2023.3252519.

[8] L. Tian, L. Cheng, J. Guo, and K. Wu, "System modeling and optimal dispatching of multi-energy microgrid with energy storage," J.

Modern Power Systems and Clean Energy, vol. 8, no. 5, pp. 809–819, 2020.

[9] Y. Jiang, C. Wan, C. Chen, M. Shahidehpour, and Y. Song, "A Hybrid Stochastic-Interval Operation Strategy for Multi-Energy Microgrids," IEEE Trans Smart Grid, vol. 11, no. 1, pp. 440–456, 2020.

[10] M. Yunshou, W. Jiekang, C. Zhihong, W. Ruidong, Z. Ran, and C. Lingmin, "Cooperative Operation Framework for a Wind-Solar-CCHP Multi-Energy System Based on Nash Bargaining Solution," IEEE Access, vol. 9, pp. 119987–120000, 2021, doi: 10.1109/ACCESS.2021.3107156.

[11] Y. Lei, X. Chen, K. Jiang, H. Li, and Z. Zou, "A Novel Methodology for Electric-Thermal Mixed Power Flow Simulation and Transmission Loss Analysis in Multi-Energy Micro-Grids," Front Energy Res, vol. 8, no. February, pp. 1–13, 2021.

[12] N. Holjevac, T. Capuder, I. Kuzle, N. Zhang, and C. Kang, "Modelling aspects of flexible multi-energy microgrids," 20th Power Systems Computation Conference, PSCC 2018, 2018.

[13] Xu D, Zhou B, Chan KW, Li C, Wu Q, Chen B, et al., "Distributed multi-energy coordination of multi-microgrids with biogas-solar-wind renewables," IEEE Trans Industr Inform 2019;15:3254–66. https://doi.org/10.1109/TII.2018.2877143.

[14] D. Qiu, T. Chen, G. Strbac, and S. Bu, "Coordination for Multi-energy Microgrids Using Multiagent Reinforcement Learning," IEEE Trans Industr Inform 2023;19:5689–700. https://doi.org/10.1109/TII.2022.3168319.

[15] Y. Cao, Y. Mu, H. Jia, X. Yu, K. Hou, and H. Wang, "A Multi-Objective Stochastic Optimization Approach for Planning a Multi-Energy Microgrid Considering Unscheduled Islanded Operation," IEEE Trans Sustain Energy, vol. 15, no. 2, pp. 1300–1314, Apr. 2024, doi: 10.1109/TSTE.2023.3341898.

[16] S. M. Nosratabadi, R. Hemmati, and P. Khajouei Gharaei, "Optimal planning of multi-energy microgrid with different energy storages and demand responsive loads utilizing a technical-economic-environmental programming," Int J Energy Res, vol. 45, no. 5, pp. 6985–7017, Apr. 2021, doi: 10.1002/er.6286.

[17] Xu D, Zhou B, Chan KW, Li C, Wu Q, Chen B, et al., "Distributed multi-energy coordination of multi-microgrids with biogas-solar-wind renewables," IEEE Trans Industr Inform 2019;15:3254–66. https://doi.org/10.1109/TII.2018.2877143.

[18] C. Zhang, Y. Xu, Z.Y. Dong, L. and F. Yang, "Multi-time-scale Coordinated Adaptive Robust Operation for Industrial Multi-energy Microgrids with Load Allocation," IEEE Trans Industr Inform 2020;16:3051–63. https://doi.org/10.1109/TII.2019.2907710.

[19] D. Qiu, T. Chen, G. Strbac, and S. Bu, "Coordination for Multi-energy Microgrids Using Multiagent Reinforcement Learning," IEEE Trans Industr Inform 2023;19:5689–700. https://doi.org/10.1109/TII.2022.3168319.

[20] Y. Mao et al., "A Collaborative Demand-Controlled Operation Strategy for a Multi-Energy System," IEEE Access, vol. 9, pp. 80571–80581, 2021, doi: 10.1109/ACCESS.2021.3083922.

[21] Y. Zhuang, Y. Liu, Z. Rong, and J. Chen, "Flexibility Exploitation With Nonlinear Integrated Demand Response for Multi-Energy System Against Load Estimation Mistake," IEEE Access, vol. 11, pp. 35579–35590, 2023, doi: 10.1109/ACCESS.2023.3266056.

[22] N. B. Roy and D. Das, "Probabilistic optimal power allocation of dispatchable DGs and energy storage units in a reconfigurable grid-connected CCHP microgrid considering demand response," J Energy Storage, vol. 72, Nov. 2023, doi: 10.1016/j.est.2023.108207.

[23] Q. Y. Wang, X. L. Lv, and A. Zeman, "Optimization of a multi-energy microgrid in the presence of energy storage and conversion devices by using an improved gray wolf algorithm," Appl Therm Eng, vol. 234, Nov. 2023, doi: 10.1016/j.applthermaleng.2023.121141.

[24] K. Kumar, and S. Bae, "Dynamic power management based on model predictive control for hybrid-energy-storage-based grid-connected microgrids," International Journal of Electrical Power and Energy Systems 2022;143. https://doi.org/10.1016/j.ijepes.2022.108384.

[25] Q. Zhang, X. Chen, G. Li, J. Feng, and A. Yang, "Model Predictive Control Method of Multi-Energy Flow System Considering Wind Power Consumption," IEEE Access, vol. 11, pp. 86697–86710, 2023, doi: 10.1109/ACCESS.2023.3304697.

[26] A. Chaouachi, R. M. Kamel, R. Andoulsi, and K. Nagasaka, "Multiobjective intelligent energy management for a microgrid," IEEE Transactions on Industrial Electronics, vol. 60, no. 4, pp. 1688–1699, 2013, doi: 10.1109/TIE.2012.2188873.

[27] K. Li, and K. J. Tseng, "Energy efficiency of lithium-ion battery used as energy storage devices in micro-grid," in: IECON 2015 - 41st Annual Conference of the IEEE Industrial Electronics Society, Institute of Electrical and Electronics Engineers Inc., 2015, pp. 5235–5240, https://doi.org/10.1109/IECON.2015.7392923.

[28] Solar Institut Jülich, CARNOT – Conventional And Renewable eNergy CARNOT – Conventional And Renewable Energy Systems OptimizationToolbox.

[29] S. Lohmann, "Einführung in die Software MATLAB® - Simulink® und die Toolboxen CARNOT und Stateflow® zur Simulation von Gebäude- und Heizungstechnik,"

[30] W. The MathWorks, Inc. "PV Array" mathworks.com. Accessed: May 04, 2024. [Online]. Available: https://es.mathworks.com/help/sps/powersys/ref/pvarray.html.

[31] Z. Lang, and Y. Zhang, "Parameter identification and performance estimation for PV modules based on reduced forms model," J Renew Sustain Energy 2020;12(5): 053703. https://doi.org/10.1063/5.0019511.

[32] SimPowerSystems TM. Reference. Natick, MA: Hydro-Quebec and the MathWorks. Inc; 2015.

[33] B. Maroua, Z. Laid, H. Benbouhenni, M. Fateh, N. Debdouche, and I. Colak, "Robust type 2 fuzzy logic control microgrid-connected photovoltaic system with battery energy storage through multi-functional voltage source inverter using direct power control," Energy Reports, vol. 11, pp. 3117–3134, Jun. 2024, doi: 10.1016/j.egyr.2024.02.047.

[34] W. Dong, Q. Yang, X. Fang, and W. Ruan, "Adaptive optimal fuzzy logic based energy management in multi-energy microgrid considering operational uncertainties," Appl Soft Comput, vol. 98, Jan. 2021, doi: 10.1016/j.asoc.2020.106882.

[35] A. C. Duman, H. S. Erden, Ö. Gönül, and Ö. Güler, "A home energy management system with an integrated smart thermostat for demand response in smart grids," Sustain Cities Soc, vol. 65, Feb. 2021, doi: 10.1016/j.scs.2020.102639.

[36] M. Arora, G. M. Vishwanath, A. Sharma, and N. Chilamkurti, "A Novel Price Discovery Insurance Scheme for Outage Resilient Energy Management System," IEEE Trans Ind Appl, 2023, doi: 10.1109/TIA.2023.3339471.

Pablo Horrillo-Quintero was born in Medina Sidonia, Cádiz, Spain, in 1997. He received the B.Sc degree in Electrical Engineering and the M.Sc degree in Renewable Energies and Energy Efficiency from the University of Cadiz in 2020 and 2021, respectively. Since 2022, he is a Research Fellow with the Research Group in Sustainable and Renewable Electrical Technologies. His-current research interests include dynamic modelling, multi-energy microgrids, renewable systems, power converters and control.

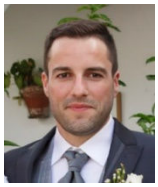

Pablo García-Triviño was born in La Línea de la Concepción, Cádiz, Spain, in 1984. He received the B.Sc. degree in Electrical Engineering, the M.Sc. degree in Industrial Engineering and the Ph.D. degree from the University of Cádiz, Cádiz, in 2005, 2007 and 2010, respectively. Since 2008, he has been an Associate Professor with the Department of Electrical Engineering, University of Cádiz. His current research interests include power systems and power management in hybrid systems.

Ehsan Hosseini was born in Isfahan, Iran. He received the Ph.D. degree from the University of Cádiz, in 2023. His current research interests include reinforcement learning for power systems control, smart grids, microgrids, renewable systems, and power converters.

Carlos. A García-Vázquez was born in La Línea de la Concepción, Spain. He received the M.Sc. degree in engineering and Ph.D. degree from the University of Cadiz, in 2004 and 2009, respectively. Since 1988, he has been with the Department of Electrical Engineering, University of Cadiz, Algeciras, Spain. Currently he is Associate Professor in this Department. His research interest focuses on electric machines, renewable energy and smart grids.

Higinio Sánchez-Sainz (Senior Member, IEEE) received the Ph.D. degree in Industrial Engineering from National University of Education at Distance UNED (Spain) in 2005. He is currently an Associate Professor with University of Cadiz (Spain). His research interests include renewable energy, electric drive, and microgrids.

Carlos E. Ugalde-Loo (Senior Member, IEEE) was born in Mexico City. He received the Ph.D. degree in electronics and electrical engineering from the University of Glasgow, Scotland, U.K.In 2010, he joined the School of Engineering, Cardiff University, Wales, U.K., where he is currently a Professor of electrical power systems and the Group Leader of the Centre for Integrated Renewable Energy Generation and Supply. His academic expertise includes power system stability and control, grid integration and control of renewables, dc transmission, modeling and control of integrated energy systems, and multi-variable control.

Vedran S. Perić (Member, IEEE) Ph.D. degree from the KTH Royal Institute of Technology, Stockholm, Sweden (primary institution), the Delft University of Technology, Delft, The Netherlands, and Comillas Pontifical University, Madrid, Spain, in 2016. He is currently an Associate Professor at Aarhus University, Denmark. His research interests include power system operation and control, with the focus on commercial application of innovative technologies.

Luis M. Fernández-Ramírez (Senior Member, IEEE) was born in Los Barrios, Cadiz, Spain. He received the M.Sc. degree in Electrical Engineering from the University of Seville, Seville, Spain, in 1997, and the Ph.D. degree from the University of Cadiz, Cadiz, in 2004. He is currently a Full Professor with the Department of Electrical Engineering and the Head of the Research Group in Sustainable and Renewable Electrical Technologies (PAIDI-TEP023). His research interests include smart grids, microgrids, renewable energy, energy storage, hydrogen systems, electrical transport systems, smart energy, multi-energy systems, power converters and control.